A&A 419, 25–34 (2004)
DOI: 10.1051/0004-6361:20034218

Astronomy & Astrophysics

The continuum spectral features of blazars in the optical region

M. Fiorucci[1,2,3], S. Ciprini[1,2], and G. Tosti[1,2]

[1] Astronomical Observatory and Physics Department, University of Perugia, via Pascoli, 06123 Perugia, Italy
[2] INFN, Sezione di Perugia, via A. Pascoli, 06123 Perugia, Italy
[3] INAF – Osservatorio Astronomico di Padova, Sede di Asiago, via Osservatorio 8, 36012 Asiago (VI), Italy

Received 21 August 2003 / Accepted 29 December 2003

Abstract. Many quasi-simultaneous optical observations of 37 blazars were obtained at the Perugia University Observatory over the last ten years. In this paper we analyze the dereddened spectral flux distribution in the optical frequency range, and we compare our results with the overall spectral energy distribution (SED). The implications for existing models of the objects are briefly discussed. In particular, we show how the LBLs have a spectral slope $\alpha \simeq 1.5$, as expected from Synchrotron Self-Compton models, while the optical emission of HBLs and FSRQs is probably contaminated by other components. Moreover, we show evidence of how the spectral index vs. flux plot exhibits a characteristic loop-like pattern that is probably due to changes in the injection of accelerated particles.

Key words. galaxies: active – galaxies: BL Lacertae objects: general – galaxies: quasars: general

1. Introduction

Blazars are a subclass of active galactic nuclei (AGN) that include BL Lac objects (BL Lacs) and flat-spectrum radio Quasars (FSRQs). Their observable characteristics are usually explained with the same physical mechanism: beamed emission from a relativistic jet aligned with our line of sight. The spectral energy distribution (SED) of BL Lacs from the radio to the X-ray range is dominated by non-thermal emission due to synchrotron radiation. FSRQs show also strong emission lines and a thermal contribution that may be comparable to the synchrotron emission in the optical spectral region. Figure 1 shows the radio to γ-ray SED of a few blazars in our dataset.

The study of SED properties is an excellent diagnostic tool for theoretical models. There is a handful of very interesting information related to the physical properties of the emitting region. However, as far as variability is concerned, many emission models are still unable to reproduce and predict the variability features observed in every region of the spectra. Recently, the internal shock model described by Spada et al. (2001) has made predictions on variability which can be compared with observations, but the availability of the simultaneous multi-wavelength observations is generally inadequate to trace the time evolution for both the synchrotron and inverse Compton components. All is simpler if the time evolution is neglected and the average SED is considered. During the past 20 years, many authors have considered the overall SED (e.g. Landau et al. 1986; Brown et al. 1989) in order to identify continuity properties and systematic trends as a function of physical or observational parameters. Even in the case of Fig. 1, where we have superimposed asynchronous data, it is possible to identify some continuity. The overall spectral shape seems to change smoothly and continuously along the $\alpha_{\rm RX}$ sequence (Ghisellini et al. 2002).

A different kind of simplification is obtained by considering time evolution in a selected region of the spectra, for example in the optical. The optical region is very narrow with respect to other spectral regions, nevertheless it may yield a large amount of information if there is a large dataset to analyze. In this case, the complication is the possible presence of other components in addition to the synchrotron continuum. For example, thermal emission from the accretion disk around the central engine, the emission from the surrounding regions of the nucleus, the host galaxy contribution. The purpose of this paper is to list and analyze the main features of the optical SED for an extended sample of blazars, primarily composed of BL Lac Objects. We report on quasi-simultaneous ($\Delta t < 2$ h) $BVR_{\rm c}I_{\rm c}$ observations of 37 blazars obtained in the course of ten years of systematic monitoring at the Perugia Astronomical Observatory. This is an important contribution to the overall SED database for many of the selected blazars. From a statistical analysis of the optical spectral continuum we derive information on the characteristics of this class of objects, and constrain theoretical models.

The structure of the paper is as follows. In Sect. 2 we describe how the data were collected and treated. In Sects. 3 and 4 the general characteristics of the optical spectral flux distributions are outlined and compared with the existing SED catalogs. In Sect. 5 we discuss the results with respect to the existing theoretical models, and our conclusions are presented in Sect. 6.

Send offprint requests to: M. Fiorucci,
e-mail: Massimo.Fiorucci@pg.infn.it

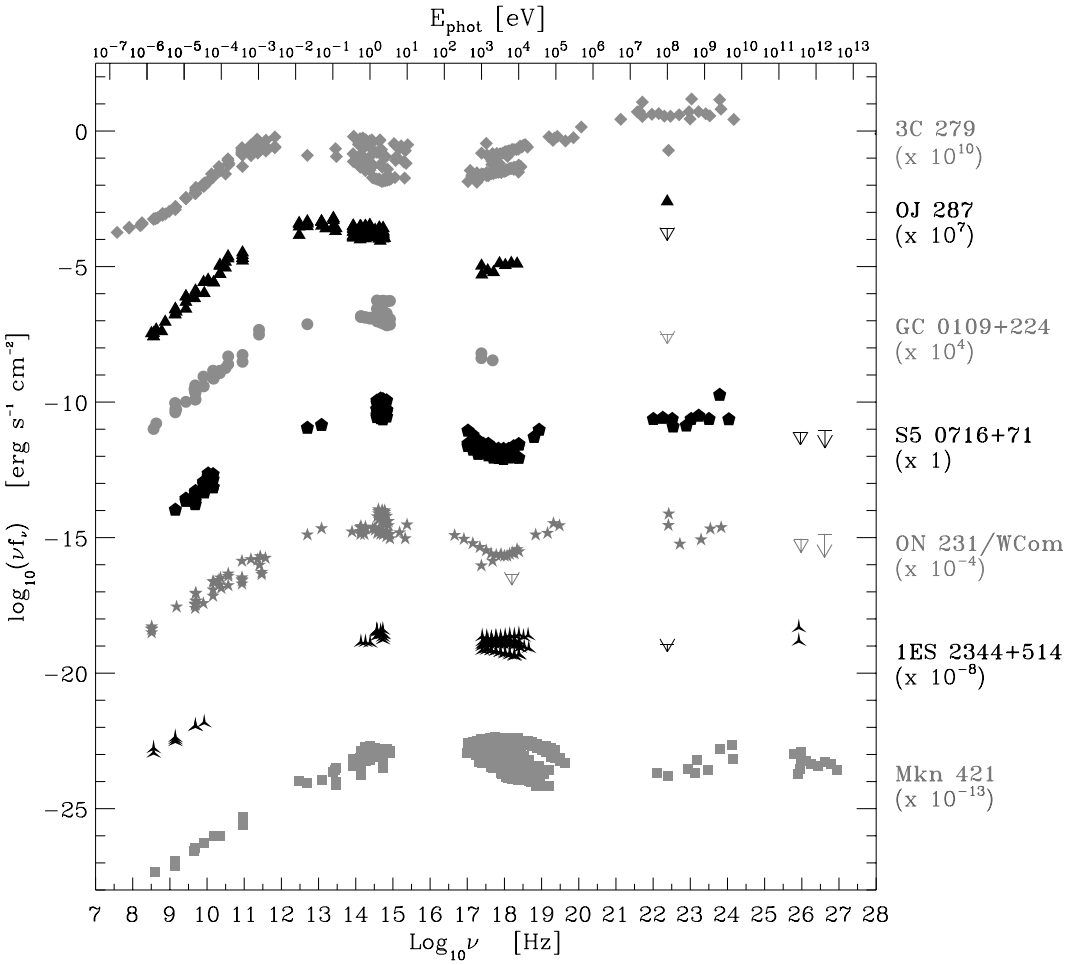

Fig. 1. The overall spectral power distribution of sample blazars. Errors bars are not reported for clarity. Multiwavelength data are not simultaneous, and correspond to different emission states of every source. Data are taken mainly from Giommi et al. (2002), NED, and Simbad databases. The optical part of the spectrum is updated including some representative data from our database (e.g. higher, average and lower states). Shown in the upper part of the plot are the SED of 3C 279 (PKS 1253−05, z = 0.5362) a typical FSRQ (data also from Reuter et al. 1997; Wehrle et al. 1998), and the SED of OJ 287 (PG 0851+202, z = 0.306), a typical LBL (data also from Idesawa et al. 1997; Massaro et al. 2003). Shown in the mid part of the plot are the SEDs of three LBL-intermediate blazars: GC 0109+224 (S2 0109+22, $z > 0.4$, data from Ciprini et al. 2004), S5 0716+71 (1H 0717+714, $z > 0.3$, data also from Tagliaferri et al. 2003), and W Comae (ON 231, z = 0.102, data also from Tagliaferri et al. 2000). In the lower part of the plot, the SEDs of two typical HBL and TeV-blazars: 1ES 2344+514 (z = 0.044), and Mrk 421 (B2 1101+38, z = 0.03, data also from Takahashi et al. 2000; Maraschi et al. 1999).

2. Observations

The data analyzed in this paper were obtained at the Perugia University Observatory with the 0.40 m Automatic Imaging Telescope (AIT, Tosti et al. 1996). The observations started in 1992, and the instrument has been fully automatic since October 1994. The AIT is still observing more than 40 blazars in the VR_cI_c Johnson-Cousins bands. The Johnson B band is also used, but only for the brightest sources. The exposure integration times vary from 3 to 8 min, according to the brightness of the object and the observing conditions. Therefore the duration of each photometric run during good weather conditions is always less than 1 h for each blazar.

Each CCD image is processed by an automatic procedure which performs dark current and bias correction, field recognition, star finding, evaluation of comparison stars and blazar instrumental magnitudes with a typical aperture radius of 4 arcsec. Instrumental magnitudes are then converted to standard Johnson-Cousins magnitudes using the sequences of stars reported in Fiorucci (1995), Fiorucci & Tosti (1996), and Fiorucci et al. (1998). A comparison with other published sequences shows a general agreement within typical standard deviations (Smith & Balonek 1998; Webb & Malkan 2000; Gonzalez-Perez et al. 2001).

A more complete description of the data collection will be available in Tosti et al. (in preparation), where all the BVR_cI_c magnitudes will be reported. Including the latest observations, the dataset contains a total of more than 20 000 photometric data. Our experience is that the number of observations performed with the Perugia robotic telescope is at least one order of magnitude greater than the number achieved with a standard manual procedure. This is evidence for the importance of robotic telescopes in blazar monitoring. In addition, the quality of the results is not degraded by the automatic

Table 1. List of the selected blazars. Columns 2–5 contain names and information as reported by Véron-Cetty & Véron (2001). Column 6 gives the interstellar coefficient used in this paper. The last columns contain the radio-to-X ray spectral index and the blazar class.

IAU name (B1950)	Common name	Coordinates (J2000) α	δ	z	A_V	α_{RX}	Class
0109+224	S2 0109+22	01 12 05.8	+22 44 39	>0.40	0.124	0.86	LBL
0219+428	3C 66A	02 22 39.6	+43 02 08	0.444	0.279	$0.78^{\pm0.07}$	LBL
0235+164	AO 0235+164	02 38 38.9	+16 37 00	0.940	0.265	$0.89^{\pm0.07}$	LBL
0300+470	4C 47.08	03 03 35.2	+47 16 17		0.870	0.92	LBL
0316+413	NGC 1275	03 19 48.2	+41 30 42	0.017	0.540	0.84	
0323+022	2E 0323+0214	03 26 13.9	+02 25 14	0.147	0.372	$0.55^{\pm0.07}$	HBL
0414+009	2E 0414+0057	04 16 52.4	+01 05 24	0.287	0.393	$0.54^{\pm0.01}$	HBL
0422+004	PKS 0422+00	04 24 46.8	+00 36 07		0.335	0.87	LBL
0716+714	S5 0716+71	07 21 53.3	+71 20 36	>0.30	0.102	$0.82^{\pm0.03}$	LBL
0735+178	PKS 0735+17	07 38 07.4	+17 42 19	>0.42	0.116	$0.92^{\pm0.02}$	LBL
0754+100	PKS 0754+100	07 57 06.7	+09 56 35	0.280	0.075	$0.84^{\pm0.02}$	LBL
0806+524	1ES 0806+524	08 09 49.2	+52 18 58	0.138	0.147	0.59	HBL
0829+046	PKS 0829+046	08 31 48.9	+04 29 39	0.180	0.108	$0.86^{\pm0.01}$	LBL
0851+202	OJ 287	08 54 48.8	+20 06 30	0.306	0.094	$0.81^{\pm0.03}$	LBL
0912+297	B2 0912+29	09 15 52.4	+29 33 24		0.081	$0.71^{\pm0.02}$	HBL
0954+658	S4 0954+65	09 58 47.2	+65 33 54	0.367	0.380	$0.90^{\pm0.01}$	LBL
1101+384	Mrk 421	11 04 27.2	+38 12 32	0.031	0.051	$0.56^{\pm0.03}$	HBL
1147+245	OM 280	11 50 19.2	+24 17 54	>0.20	0.090	$0.92^{\pm0.06}$	LBL
1215+303	ON 325	12 17 52.1	+30 07 01	0.130	0.079	$0.75^{\pm0.02}$	HBL
1219+285	ON 231 (W Com)	12 21 31.7	+28 13 58	0.102	0.075	$0.81^{\pm0.07}$	LBL
1226+023	3C 273	12 29 06.7	+02 03 08	0.158	0.068	$0.85^{\pm0.10}$	FSQ
1253−055	3C 279	12 56 11.1	−05 47 21	0.538	0.095	$0.93^{\pm0.03}$	FSQ
1415+259	2E 1415+2557	14 17 56.6	+25 43 25	0.237	0.062	$0.55^{\pm0.02}$	HBL
1418+546	OQ 530	14 19 46.6	+54 23 14	0.152	0.044	$0.87^{\pm0.02}$	LBL
1424+240	PKS 1424+240	14 27 00.5	+23 48 00		0.194	$0.70^{\pm0.01}$	HBL
1458+228	MS 14588+2249	15 01 01.9	+22 38 06	0.235	0.159	$0.59^{\pm0.12}$	HBL
1611+343	DA 406	16 13 41.0	+34 12 48	1.404	0.060	0.92	FSQ
1641+399	3C 345	16 42 58.8	+39 48 37	0.594	0.044	$0.91^{\pm0.01}$	FSQ
1652+398	Mrk 501	16 53 52.2	+39 45 36	0.033	0.064	$0.63^{\pm0.05}$	HBL
1722+119	H 1722+119	17 25 04.4	+11 52 16	0.159	0.568	$0.50^{\pm0.08}$	HBL
1727+502	I Zw 187	17 28 18.6	+50 13 11	0.055	0.098	$0.61^{\pm0.02}$	HBL
1807+698	3C 371	18 06 50.7	+69 49 28	0.050	0.119	$0.83^{\pm0.06}$	LBL
2032+107	PKS 2032+107	20 35 22.0	+10 56 06	0.601	0.474	$0.80^{\pm0.08}$	LBL
2200+420	BL Lac	22 02 43.3	+42 16 39	0.069	1.091	$0.84^{\pm0.04}$	LBL
2251+158	3C 454.3	22 53 57.7	+16 08 54	0.859	0.355	$0.89^{\pm0.01}$	FSQ
2254+074	PKS 2254+074	22 57 17.3	+07 43 12	0.190	0.219	$0.91^{\pm0.03}$	LBL
2344+514	1ES 2344+514	23 47 04.8	+51 42 18	0.044	0.716	$0.60^{\pm0.02}$	HBL

procedures: our data are generally in agreement with the magnitudes measured on the same nights with traditional telescopes (see, e.g., Massaro et al. 1996; Takalo et al. 1996; Raiteri et al. 1999; Tosti et al. 2002).

3. Characteristics of the dataset

Table 1 reports the object list, sorted by increasing right ascension. Column 1 reports the IAU name. Columns 2–5 give the source designation, the coordinates and the redshift as indicated by Véron-Cetty & Véron (2001).

The photometric data, obtained at the Perugia Astronomical Observatory up to the end of 2002, were corrected for galactic interstellar reddening using the extinction values A_V listed in Col. 6. They were deduced from the maps of dust infrared emission reported by Schlegel et al. (1998). The same authors declare that the maps have an accuracy of 16% in predicting reddening. Other extinction values can be found in the literature or deduced from the hydrogen column density (Elvis et al. 1989), but we used the same estimation for homogeneity. In addition, the values of A_V estimated from the hydrogen column density are not very accurate, with a typical uncertainty of the order of 25–30% (Bersanelli et al. 1992). From the A_V values, we have obtained the extinction values at the other wavelengths using the curve of Cardelli et al. (1989).

The last columns in Table 1 are devoted to a first classification of the blazars. For the sake of order, we can divide the blazar class into three sub-types characterized by different

average properties (Padovani & Giommi 1995). FSRQs are the quasar-like blazars, so they can be identified by strong emission lines. High-energy-peak BL Lacs (HBL) are BL Lacs that predominantly emit synchrotron power at high frequencies (UV-X), and can be selected empirically with $\alpha_{\rm RX} \leq 0.75$[1]. Low-energy-peak BL Lacs (LBL) are BL Lacs that emit most of their synchrotron power at low frequencies (IR-Opt), and can be selected with the rule: $\alpha_{\rm RX} > 0.75$. This tentative classification is an attempt to clarify the enigmatic nature of these sources, but the distribution among these sub-types is ambiguous, as several sources show intermediate behavior. We have included in Col. 7 of Table 1 the mean $\alpha_{\rm RX}$ and the greatest reported deviations. The numbers are obtained essentially from the catalog of Donato et al. (2001), integrated with the data reported by Ledden & O'Dell (1985) and Lamer et al. (1996). Finally, Col. 8 reports the adopted classification. There is no general agreement about the classification of NGC 1275; this source has been called, at various times and not always by different astronomers, a Seyfert galaxy, a radio galaxy, or a blazar. We have therefore omitted this classification, but it will be considered a FSRQ during the following analysis.

Our dataset contains 18 LBLs, 13 HBLs, and 6 FSRQs (or sources which have strong thermal contributions at optical wavelengths). It is easy to verify that our sample of blazars is biased toward the BL Lac Objects. This is partially due to the fact that photometric broad-band analysis is easier for this class of sources, thanks to the relative absence of lines in their spectrum. Moreover with our small-size telescope we have selected blazars that are optically bright. In many cases this means we are looking at a sample of sources with the synchrotron emission peaked in the optical.

4. The optical spectral flux distribution

The optical flux densities (expressed in mJy) were obtained from the dereddened standard magnitudes using the conversion factors reported by Bessell (1979). From the same author we have adopted the effective wavelengths corresponding to the $BVR_{\rm c}I_{\rm c}$ broad bands, neglecting the changes due to the different spectra of the observed sources. Of the large dataset collected at the Perugia Astronomical Observatory, we considered only the flux densities measured with $S/N > 15$, to exclude the poor quality data that can wrongly influence the analysis. The value of 15 is a compromise between the need for high quality data and for data of faint blazars or of blazars during their low emission phases.

With the data resulting from this first selection, we have analyzed the presence of a power law $f(\nu) \propto \nu^{-\alpha}$ searching for linear fits on a $\log \nu - \log f(\nu)$ scale. The assumption is that the dereddened spectral flux distribution in the optical range can be described by a single power law (see Figs. 2, 3). We have accepted only the data that allow us to calculate the regression based on at least three quasi-simultaneous ($\Delta t < 2$ h) photometric bands, and with the square of Pearson's linear correlation coefficient $r^2 > 0.9$. The typical standard deviation of the slope α is 0.1. This strong selection criterion cuts off all the sets of three-four data that contain at least one wrong value, or the cases where there is an "anomalous" change in slope. However, these cases were individually re-analyzed to verify the presence of a *real* curvature in the spectral flux distribution, and the existence of some deterministic relation between the changes in slope and the blazar state. We have verified that the

[1] The radio-to-X ray spectral index is defined: $\alpha_{\rm RX} = -0.13 \log(F_{1\ \rm KeV}/F_{5\ \rm GHz})$.

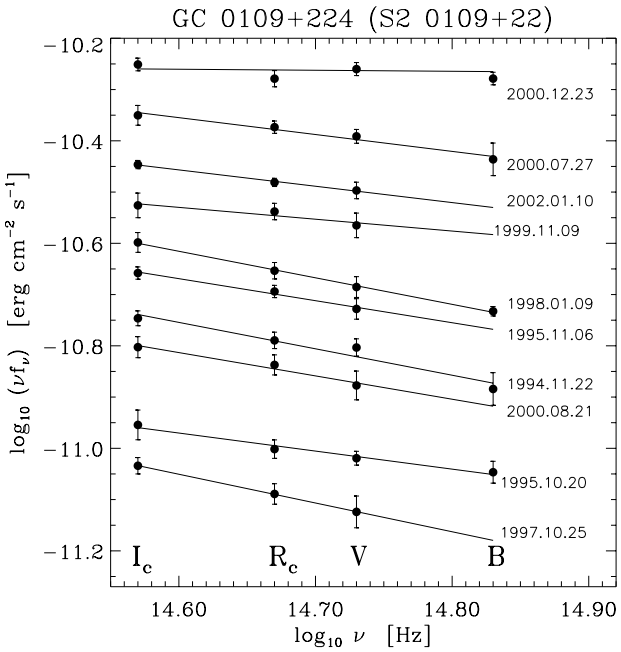

Fig. 2. The spectral power distribution of 0109+224 in the optical region with a selection of different continuum spectra. The spectral region is so narrow that it is plausible to describe it by a single power law. A weak flattening with increasing flux is visible (Ciprini et al. 2003).

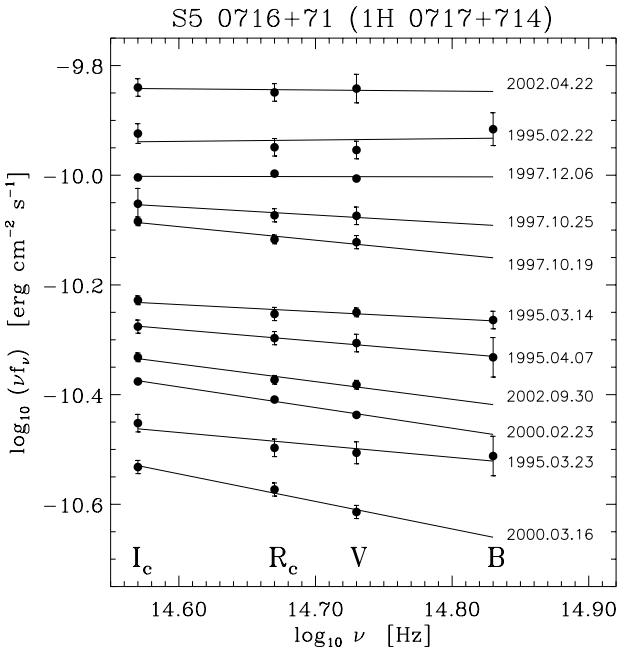

Fig. 3. The spectral power distribution of 0716+714 in the optical region, with a selection of different continuum spectra.

Table 2. Flux density and spectral slope in the optical region. The average flux density, the extreme values (minimum and maximum), and the number of data used are reported for each filter. For the spectral slope α we added the standard deviation, and the skewness index with respect to the Gaussian distribution.

Source	B [mJy]			V [mJy]			R_c [mJy]			I_c [mJy]			α			
	ave	ext	N	ave	ext	N	ave	ext	N	ave	ext	N	average	ext	N	skew
0109+224	4.36	1.94 5.80	5	3.64	1.30 9.52	148	4.51	1.61 10.72	148	6.11	2.49 14.22	148	1.41 ± 0.18	2.11 0.85	148	−0.2
0219+428	9.49	2.59 17.11	66	8.88	2.59 18.91	218	10.61	4.04 22.42	217	13.93	5.58 28.50	217	1.22 ± 0.19	1.94 0.72	218	−0.6
0235+164				0.76	0.39 1.26	8	1.01	0.53 1.96	8	1.82	0.94 3.52	8	2.37 ± 0.31	2.70 1.79	8	+0.8
0300+470				2.24	1.21 3.51	20	3.03	1.75 4.30	20	4.15	2.33 6.36	20	1.57 ± 0.42	2.28 0.79	20	+0.5
0316+413	10.96	8.54 15.26	48	14.32	12.05 17.42	67	18.82	16.24 21.31	67	21.57	19.00 25.75	67	1.07 ± 0.17	1.34 0.52	67	+1.1
0323+022				1.03	0.90 1.17	7	1.21	1.00 1.40	7	1.50	1.26 1.74	7	1.01 ± 0.10	1.19 0.87	7	−0.4
0414+009				1.27	0.76 1.65	6	1.40	0.83 1.81	6	1.60	0.96 2.03	6	0.59 ± 0.13	0.78 0.45	6	−0.2
0422+004	11.33	9.27 13.90	4	8.19	2.13 20.47	138	9.94	2.95 24.52	138	12.85	3.84 30.52	138	1.24 ± 0.19	1.89 0.84	138	−0.6
0716+714	9.24	4.26 18.06	13	10.50	4.23 25.00	197	12.67	5.74 30.41	197	16.90	7.93 40.51	196	1.30 ± 0.18	1.98 0.90	197	−0.7
0735+178				2.47	1.13 4.61	55	2.94	1.42 5.29	55	3.90	1.90 7.23	55	1.24 ± 0.16	1.63 0.85	55	+0.3
0754+100				2.32	1.47 3.56	9	2.79	1.95 4.11	9	3.92	2.61 5.71	9	1.44 ± 0.14	1.68 1.20	9	0.0
0806+524				2.25	1.60 3.28	62	2.67	1.86 3.93	62	3.27	2.48 4.77	62	1.00 ± 0.22	1.55 0.54	62	0.0
0829+046	2.87	2.37 3.65	3	3.24	1.64 6.24	57	4.29	2.21 8.57	57	5.97	3.57 11.11	57	1.66 ± 0.19	2.09 1.22	57	−0.1
0851+202	5.01	3.40 6.36	14	3.96	0.94 8.78	276	4.89	1.15 10.21	276	7.04	1.51 14.51	276	1.59 ± 0.22	2.47 0.88	276	−0.3
0912+297				2.25	2.06 2.45	4	2.80	2.55 3.15	4	3.72	3.54 3.97	4	1.32 ± 0.16	1.52 1.15	4	−0.2
0954+658				1.90	0.92 3.23	46	2.50	1.33 4.41	46	3.43	1.82 5.96	46	1.57 ± 0.31	2.47 1.00	46	−0.8
1101+384	19.68	9.65 36.01	45	24.71	14.77 43.80	128	29.22	18.44 49.86	131	37.30	23.07 63.54	132	1.14 ± 0.16	1.68 0.84	132	−0.6
1147+245				1.15	0.72 1.56	13	1.37	0.87 1.93	13	1.99	1.11 2.62	13	1.48 ± 0.32	1.98 0.86	13	+0.3
1215+303	5.22	4.69 5.74	2	5.76	4.14 7.39	17	6.58	4.73 8.30	17	8.15	5.62 9.95	17	0.93 ± 0.14	1.25 0.70	17	−0.4
1219+285	5.86	2.30 8.81	27	8.79	2.97 34.87	299	10.52	3.63 39.25	299	13.71	4.98 47.84	299	1.24 ± 0.17	1.87 0.70	299	−0.1
1226+023				24.78	23.78 29.94	17	26.19	24.63 32.17	17	30.86	27.24 37.95	17	0.63 ± 0.12	0.76 0.32	17	+1.2
1253−055				3.98	2.51 6.01	7	5.18	2.89 8.26	7	8.26	4.94 11.00	7	1.98 ± 0.29	2.30 1.45	7	+0.6
1415+259				0.66	0.54 0.79	8	0.86	0.77 1.07	8	1.24	1.00 1.53	8	1.70 ± 0.11	1.87 1.52	8	+0.2
1418+546				2.35	1.58 3.72	15	2.68	1.85 4.20	15	3.73	2.66 5.99	15	1.30 ± 0.19	1.53 0.85	15	+1.1
1424+240	5.49	4.06 6.26	7	6.84	5.38 9.26	108	7.79	5.94 10.05	108	9.53	7.69 12.65	108	0.89 ± 0.12	1.53 0.53	108	−1.2
1458+228				2.70	1.11 4.21	28	3.10	1.41 4.94	28	3.87	1.74 5.77	28	1.00 ± 0.22	1.41 0.60	28	0.0
1611+343				0.40	0.29 0.47	9	0.47	0.36 0.59	9	0.55	0.46 0.66	9	0.86 ± 0.26	1.32 0.51	9	−0.5
1641+399				0.93	0.80 1.11	4	1.06	0.89 1.32	4	1.32	1.18 1.66	4	0.95 ± 0.17	1.07 0.72	4	+0.6
1652+398	7.74	6.48 9.36	47	11.54	9.70 13.51	138	14.89	13.25 18.29	139	22.03	20.05 25.95	139	1.75 ± 0.14	2.20 1.38	139	−0.1
1722+119	6.79	5.13 8.44	2	7.36	4.66 12.25	89	8.69	5.60 13.93	89	10.56	6.94 16.50	89	0.96 ± 0.16	1.45 0.57	89	−0.5
1727+502				1.67	1.49 1.84	10	2.06	1.81 2.26	10	2.80	2.69 3.04	10	1.39 ± 0.16	1.68 1.16	10	−0.4
1807+698				4.74	3.95 5.56	5	6.54	5.40 7.39	5	9.34	7.58 10.86	5	1.78 ± 0.14	1.94 1.64	5	−0.2
2032+107				2.40	1.95 2.88	52	4.35	3.95 5.14	52	7.55	7.02 9.13	52	2.83 ± 0.19	3.22 2.35	52	+0.2
2200+420	20.46	4.20 41.65	21	16.86	4.63 56.54	391	22.17	6.67 69.25	391	30.14	9.81 86.62	390	1.61 ± 0.21	2.16 0.96	391	+0.2
2251+158				1.42	1.09 1.77	14	1.61	1.37 2.17	14	1.93	1.67 2.50	14	0.84 ± 0.26	1.40 0.40	14	−0.2
2254+074				1.18	0.73 1.96	14	1.56	0.98 2.46	14	2.13	1.43 2.97	14	1.56 ± 0.37	2.27 1.01	14	−0.2
2344+514				4.59	3.87 5.29	69	6.29	5.52 7.62	69	9.12	8.12 10.52	69	1.80 ± 0.17	2.20 1.36	69	0.0

spectral range and the S/N are not sufficiently large to exhibit these second-order effects.

It is worth noting that the thermal contribution of the host galaxy, if it is not negligible, may produce a steepening of the energy distribution in the optical region (see, e.g., Pian et al. 1994). Typical BL Lac host galaxies are ellipticals (Urry et al. 2000), so we expect that their emission may be significant in the near-IR. However, also the optical spectral region may be effected by this thermal contribution (Falomo et al. 1993; Scarpa et al. 2000). The host galaxy emission can be identified if the source is variable, or including in the analysis the infrared data reported in the literature, but we have preferred to give only the *observed* values. In this paper we intend to estimate the derivative of the real SED in the optical region, correcting only for the interstellar absorption of our Galaxy and mapping the overall emission of the sources in all their components.

Table 2 shows for each source and each photometric band the average flux density expressed in mJy. We have also reported the minimum and maximum values and the number of data used, which obviously is a fraction of the complete database as a result of the selection criteria explained above. The last columns are the most interesting, because they

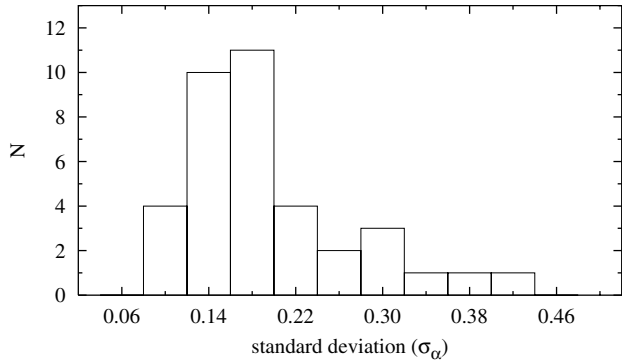

Fig. 4. Histogram of the spectral index standard deviations reported in Table 2. The average of the distribution is $\sigma_\alpha = 0.20$.

describe the average optical spectral slope α. In this case we have included the standard deviation and skewness of the distribution. Figure 4 shows the histogram of the spectral index standard deviation σ_α.

Our results on the spectral index can be compared with other similar studies. For example, Smith et al. (1987) presented optical (*UBVRI*) and near-infrared (*JHK*) photometric observations of 17 blazars; for 6 of the 8 sources in common there is a good agreement, while the results for the other two sources can be explained considering the curvature in the SED shown between the optical and the near-IR spectral regions (see also Ballard et al. 1990). Falomo et al. (1993) reported an analysis of the optical to near-infrared emission of 34 blazars, but with a different correction procedure for interstellar extinction. The spectral slopes for all 10 common sources are generally in good agreement, and always within the range of fluctuations. Fan & Lin (1996) and Fan et al. (1999) reported the compilation of the observed data for a large sample of blazars, and gave the spectral slope for many of them. Although they used *UBV* magnitudes collected from many instruments, only 4 of the 16 blazars in common have remarkable differences in the spectral slope. More recently, Vagnetti et al. (2003) analyzed the spectral slope variability of 8 BL Lacs in the BVR_cI_c bands. Our results for 7 common blazars are in perfect agreement within typical standard deviations.

5. Discussion

The dereddened spectral flux distribution in the optical wavelengths can be analyzed alone, considering the time evolution, and/or compared with the time-averaged multiwavelength SED. The point is to distinguish properly all the components that, together with the synchrotron emission, form the observed signal. What we expect to see depends on the the type of blazar, because this information tells us where the synchrotron emission is peaked.

5.1. LBLs

Optical observations play an important role in discriminating between LBLs and HBLs. In the first case, we expect to be in the descending part of the spectral power distribution, after the maximum, while in the latter case the maximum is located at higher frequencies and we are in the ascending part (see Figs. 1 and 5). Thus we expect an average spectral index $\alpha > 1$ for LBLs, and $\alpha \leq 1$ for HBLs. The histograms in Fig. 6 show that this result is confirmed for the LBLs, where the slope is always >1. As a result, in our sample α clusters around 1.5.

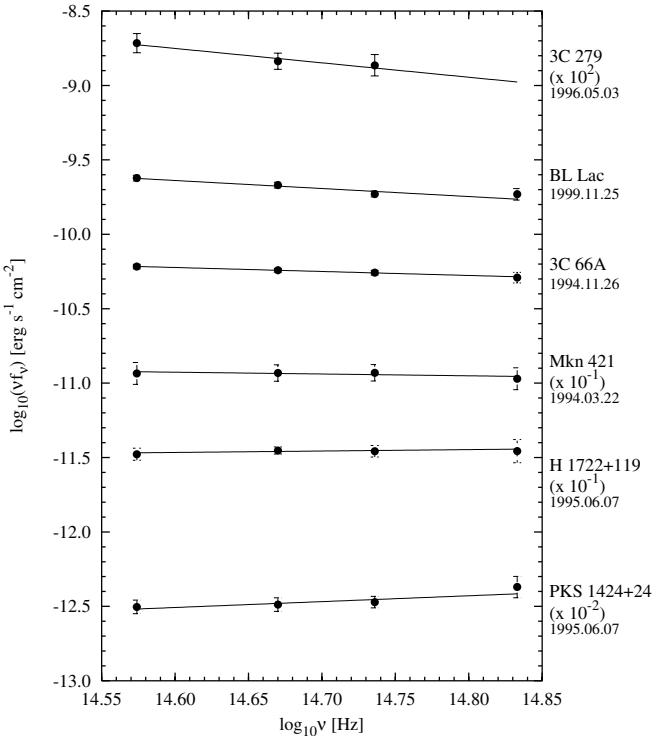

Fig. 5. Examples of optical spectral power distributions obtained with our data. Sources are ordered according to their average value of α. Note that the fluxes have been opportunely scaled to have a progressive order.

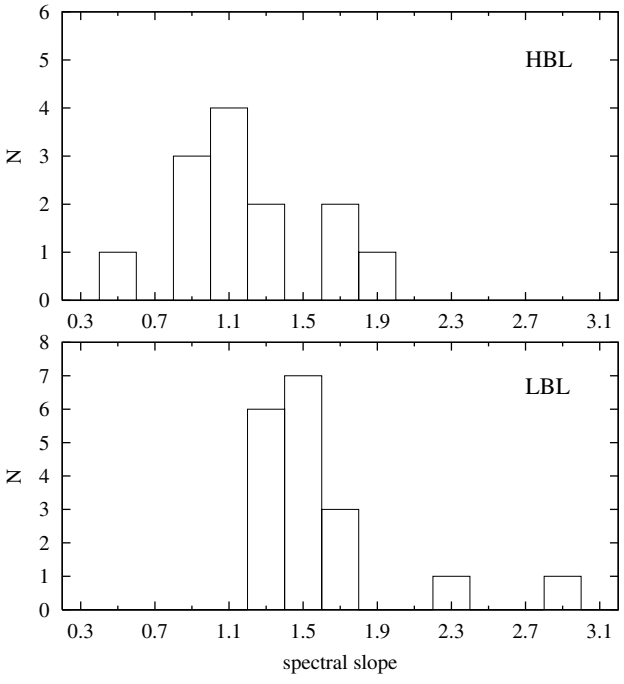

Fig. 6. Histogram of the mean spectral index for the HBLs (*top*) and LBLs (*bottom*). The average of the distribution for the LBLs is $\alpha = 1.5 \pm 0.1$, excluding the two anomalous sources PKS 2032+107 and AO 0235+164 (see the discussion of Roy et al. 2000).

For a partially cooled electron distribution, in the power-law form $N(E) = N_0 E^{-p}$, and with an isotropic pitch angle distribution, the standard emissivity for the synchrotron total spectrum is:

$$J_{\rm syn}(\nu) \propto N_0\, B^{(1+p)/2}\, \nu^{(1-p)/2}. \quad (1)$$

In the case of radiative losses dominated by Synchrotron Self Compton (SSC) emission, the time-averaged synchrotron spectrum becomes:

$$J_{\rm syn}(\nu) \propto \nu^{(1-p)/2-(4-p)/2}. \quad (2)$$

Because of the near-constant shape of the particle distribution, the synchrotron emission above the break energy $(Be\hbar\gamma^2_{\rm max})/(m_{\rm e}c^3)$ will have a roughly constant time-averaged spectral shape $F_\nu \propto \nu^{-3/2}$. Note that 16 of the 18 LBLs cluster around $\alpha \simeq 3/2$. Recently Chiang & Böttcher (2002) demonstrated that *for a broad range of particle injection distributions*, SSC-loss-dominated synchrotron emission exhibits exactly this kind of spectral slope. Thus the authors predicted a distribution of spectral indices in the optical/UV clustered around $\alpha \simeq 1.5$. From this point of view, SSC models fit very well the optical emission for LBLs, while for the HBLs we have to consider X-ray observations if we want an accurate fit.

5.2. HBLs

The fact that LBLs show an average spectral slope steeper than HBLs was expected. However, the histogram of the two classes (Fig. 6) partially overlap. The HBL spectral slope scatters in the range between 0.5 and 2.0, while we expected $\alpha \leq 1$. Therefore a classification based on the optical spectral slopes would not correspond exactly to the one adopted in Table 1. Our opinion is that the optical emission of some HBLs is contaminated by other components. This is based on two arguments:

- the SSC model reproduces very well the UV-X-γ spectral regions for HBLs, but usually does not account for radio emission, which is thought to be produced in possibly different larger regions and with longer cooling timescales. The infrared-optical spectral regions may be fitted by the model, but it is often difficult to extend their contribution to the high-energy region considering only a one-zone model;
- HBLs are generally stable in the optical. Great flares and SED changes seem to be confined to the X and γ rays (see, e.g., Pian et al. 1998). This effect may be explained if the optical emission comes from different regions of the jet, or is strongly diluted by thermal emission by the galaxy.

The host galaxy contribution is probably important at least for nearby blazars (Pian et al. 1994). For example, the spectral slope of Mrk 421 becomes $\alpha \simeq 0.85$ after the subtraction of an estimated host galaxy contribution (Tosti et al. 1998). However, it is more difficult to have a large correction for sources like 1ES 2344+514 or 2E 1415+2557.

In conclusion, the fact that the optical spectral slope of HBLs can be anywhere between 0.5 and 2.0 can be the sign of a SED deformation around the optical region for some of these blazars. Such a deformation may be due to a thermal contribution to the overall optical signal, or to non-thermal emission coming from different regions of the jet with respect to those that dominate the SED at higher frequencies.

5.3. FSRQs

The situation is similar for the FSRQs, since their optical emission is strongly contaminated by thermal emission from the accretion disk and the surrounding regions. Of particular relevance is the presence of the so-called "blue bump", or "UV bump", which flattens the spectral slope in the optical region. For example, 3C 273 clearly shows the UV bump in its SED (Türler et al. 1999) and we compute a mean optical spectral slope $\alpha \simeq 0.6$. The situation is the opposite for 3C 279, where we have $\alpha \simeq 2.0$ and the SED does not show evidence of thermal contribution (see Fig. 1 and Landau et al. 1986). Although our statistics are very poor for this type of blazars, 3C 279 is also the only FSRQ with strong variability in our sample, a fact that is generally attributed to the synchrotron emission.

5.4. Spectral slope variability

From our set of photometric measures in three or four bands, we are able to investigate possible relations between the source luminosity and the slope of the optical spectral energy distribution. The level of correlation sheds light on the non-thermal emitting processes involving synchrotron and inverse Compton cooling of the electron population in the active region.

Figure 7 shows the instantaneous spectral slope α as a function of the $R_{\rm c}$ flux density (Massaro & Trèvese 1996). The plot represents only a subset of the data, but it may be considered representative of the overall set. Strong scattering (which is only partially explainable with statistical fluctuations) is evident. The more extremely variable blazars also show a general slope-flattening trend when the source is brighter.

This phenomenon is quite common in blazars, and in the more general class of QSOs (Trevèse & Vagnetti 2002). It may be explained in different ways. For example, it may be the sign of the presence of two components that contribute to the overall emission in the optical region, one variable (with a flatter slope) and the other stable (with $\alpha_{\rm cost} > \alpha_{\rm var}$). It is also possible to explain it with a one-component synchrotron model: the more intense the energy release, the higher the particle's energy.

It is interesting to investigate the deviations. Obviously this is partially due to statistical fluctuations (see Fig. 1 in Vagnetti et al. 2003, where the signal-to-noise is generally higher). However, it is statistically impossible to explain all the fluctuations invoking only the noise: too many variations exceed 4–5 cumulative standard deviations. Progress is made if we separate the statistical distribution of the spectral slope during the *rise* and *decline* of flares. In all the well-sampled blazars it is evident that the mean slope is flatter during the rises, and steeper during the declines: for example, Figs. 8 and 9 show the statistical distributions for two blazars. This type of variability is revealed by plotting spectral index versus the flux in

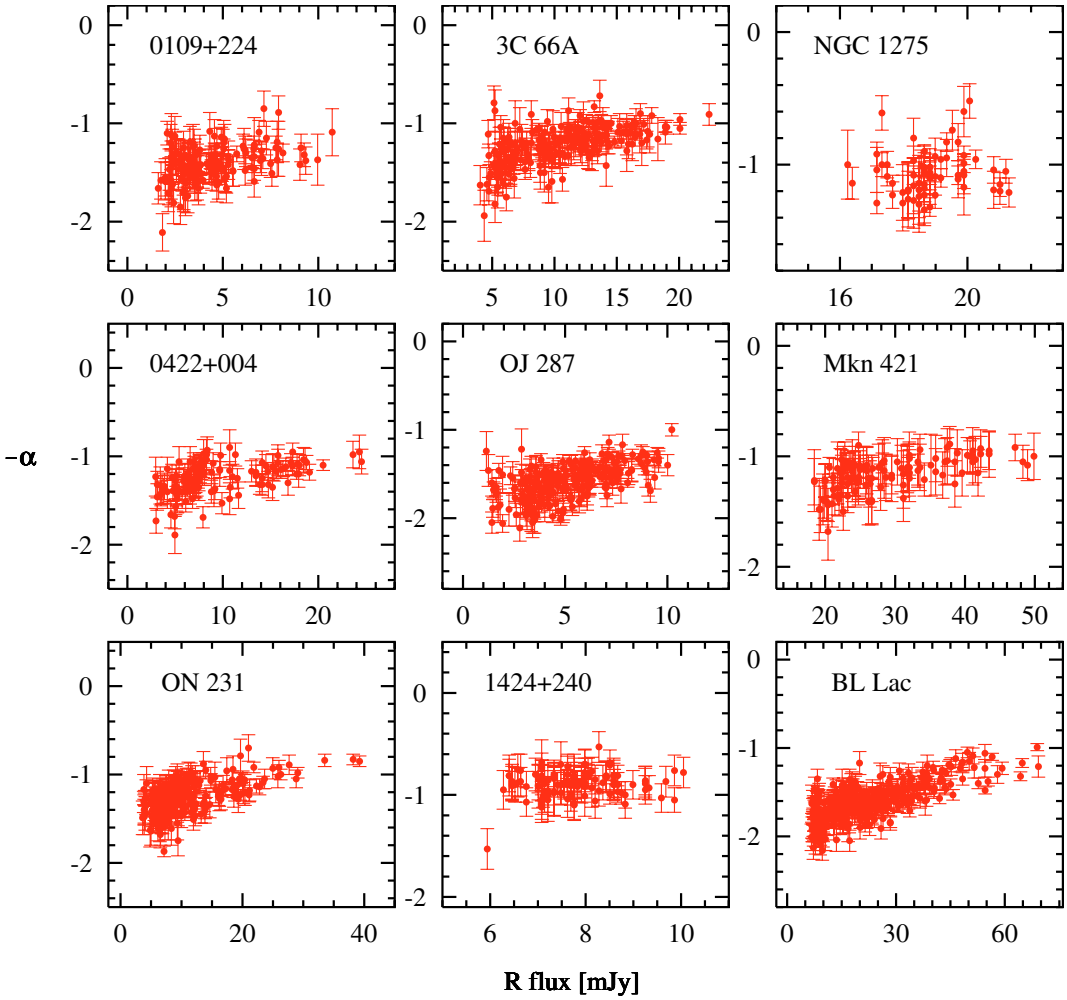

Fig. 7. Dependence of the spectral slope on intensity for a subset of blazars. The scattering, which is only partially explainable as statistical fluctuations, is evident. The more extremely variable blazars show a general trend that flattens the slope when the source is brighter.

well defined flare events. During large flares the spectral index exhibits, sometimes, a loop-like pattern that is traced in the clockwise direction (see Figs. 10–12). This type of variability pattern has been observed at shorter wavelengths in several blazars (Sembay et al. 1993; Kataoka et al. 2000), and represents a sort of hysteresis cycle in the scatter plot between the energy index and the flux. It may arise whenever the spectral slope is controlled by cooling processes (mostly synchrotron and Inverse Compton). The effects, due to changes in the injection of accelerated particles, propagate from high to low energies (Kirk et al. 1998; Kirk & Mastichiadis 1999). Only during well defined single-peaked flare events, i.e. flares that do not blend with any preceding or subsequent variability bump, is it reasonable to expect such loop-like behavior. Our data show that variability loops can be found not only in X-ray emission of blazars, but also in optical bands, if the density of observation is sufficient to correctly trace any single flux peak during outburst phases (Ciprini et al., in preparation).

6. Conclusions

Ten years of automatic optical monitoring of a sample of blazars gives us a large database and sheds light on this intriguing class of astronomical objects. In this paper we have analyzed the dereddened spectral flux distribution of 37 blazars, selecting a suitable sub-set of the quasi-simultaneous observations ($\Delta t < 2$ h). Table 2 reports the synthesis of this work; it can be used to map the optical spectral flux distribution, and to include our results within the overall SED of these objects. Optical fluxes are also useful in that they give a rough prediction of GeV gamma-ray emission, suitable for the preliminary simulation of the performances of the next generation of space gamma-ray missions (AGILE and GLAST, for example).

A discussion based on our optical data alone gives some new implications for the existing theoretical models:

- Low-frequency peaked BL Lac object are extremely variable in the optical region and their spectral slope clusters around $\alpha = 1.5$, in agreement with a Synchrotron Self-Compton model (Chiang & Böttcher 2002).
- The fact that the optical spectral slope of HBLs ranges from 0.5 to 2.0 may be the sign of a deformation of the SED for some of these sources. This deformation can be due to a thermal contribution to the overall optical signal, for example the host galaxy emission, or to non-thermal emission

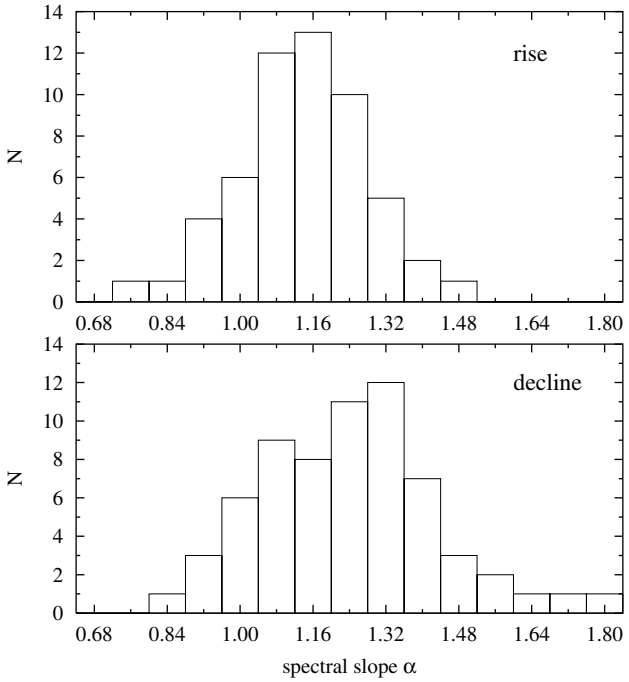

Fig. 8. Histogram of the spectral index distribution in S5 0716+71 during the rise (*top*), and decline (*bottom*). The average of the distributions is α = 1.24 and 1.38 respectively.

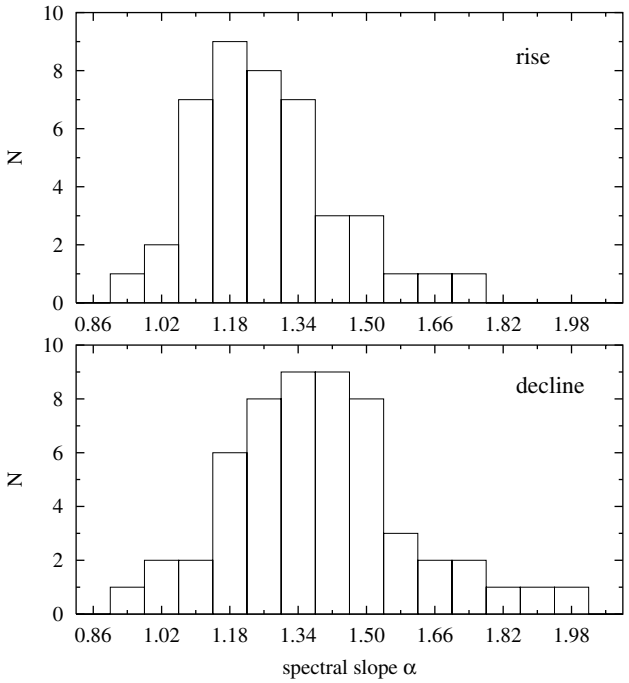

Fig. 9. Histogram of the spectral index distribution in 3C 66A during the rise (*top*), and decline (*bottom*). The average of the distributions is α = 1.15 and 1.24 respectively.

from different regions with respect to those that dominate the SED at higher frequencies.

– Many blazars show the presence of rapid fluctuations in their optical spectral slope. When it is possible to extract a single flare in the light curve, the spectral slope makes a

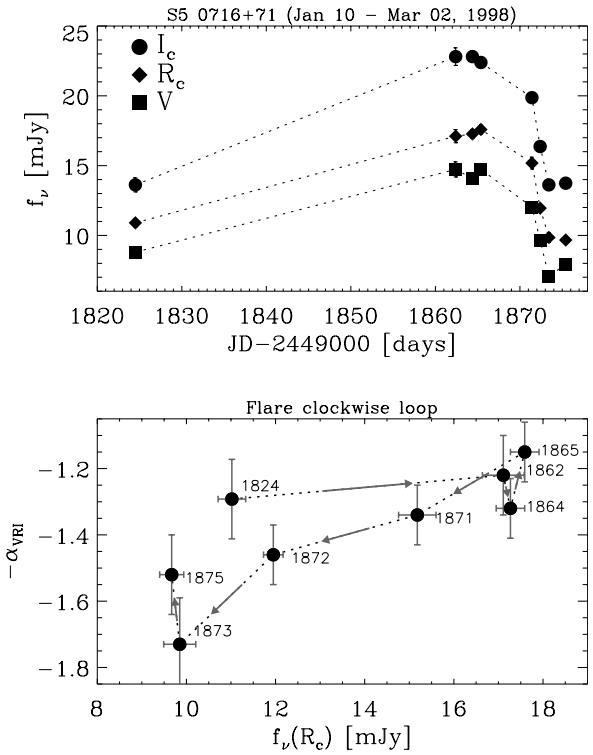

Fig. 10. Dependence of spectral slope on intensity for the first of two continuous flares of 0716+714 (the flare occurred from January 10 to March 02, 1998, *upper panel*). The spectral index during the flare describes a clockwise loop (*lower panel*). A second flare is represented in Fig. 11.

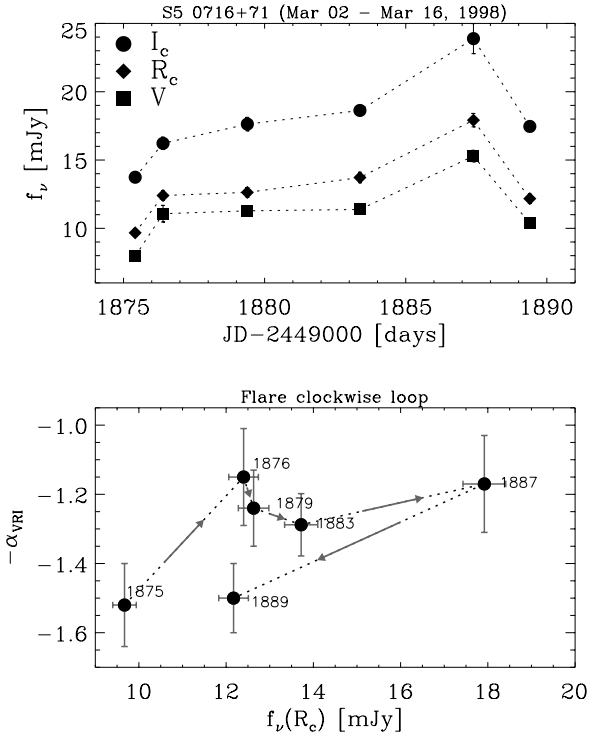

Fig. 11. Dependence of spectral slope on intensity for the second flare of 0716+714. This flare extended from March 02 to March 18, 1998 (*upper panel*). The spectral index describes again a clockwise loop (*lower panel*).

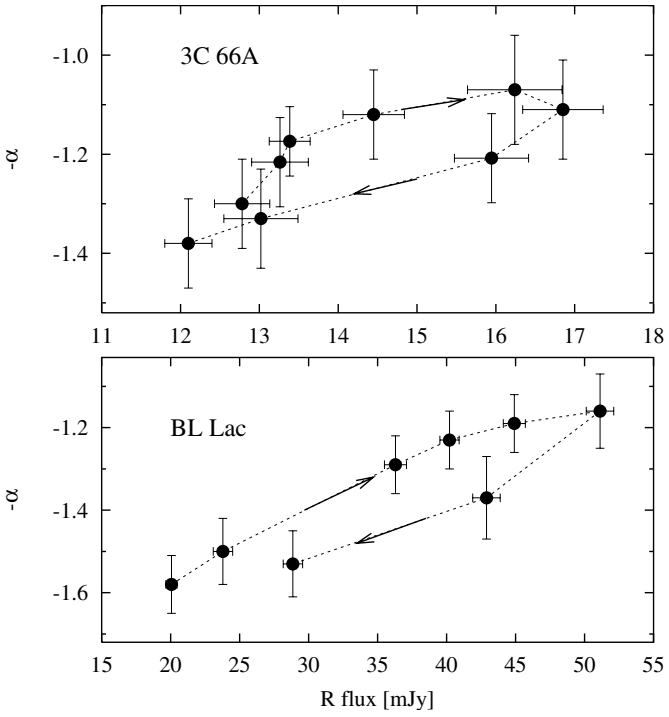

Fig. 12. Two more examples of spectral index changes during the phases of rise and decline. The data of 3C 66A refer to observations made between December 4th, 1996, and January 16th, 1997. For BL Lac, the figure shows the data from May 30th to June 16th, 2001.

loop that may be considered a feature of the synchrotron emission.

Some of these blazars show a weak but general trend toward spectral slope flattening when the source is brighter. Our data alone are not enough to distinguish if this is sign of the presence of two or more components that contribute to the overall emission in the optical, or a typical feature of a single component synchrotron source. The same problem arises when we try to comment on our data for FSRQs. We analyze the overall emission coming from the source, and it is not easy to distinguish the thermal from the non-thermal components using optical data alone. The greater part of our multiband data is obtained with only three filters (VR_cI_c), but if we want a deeper understanding of this class of objects it is essential to obtain simultaneous observations covering completely at least of the nearIR-to-optical part of the spectrum.

Acknowledgements. We are profoundly indebted to M. Bagaglia, M. Luciani, N. Marchili, G. Nucciarelli, S. Pascolini, V. Picarelli, N. Rizzi, F. Roncella, C. Spogli, and the other astronomers and technicians who during the past years worked to improve the performance of the Automatic Imaging Telescope (AIT). Many thanks to Kyle Augustson and Jet Katgert for comments and suggestions, and to Junhui Fan for his help in finding part of the bibliography. We are grateful to the referee, Dario Trèvese, for detailed and helpful comments. This research has made use of the SIMBAD database, operated by the CDS, Strasbourg, France, and of the NASA/IPAC Extragalactic Database (NED), which is operated by the Jet Propulsion Laboratory, California Institute of Technology. Part of this work has been supported by the Italian MIUR under grant Cofin2001/028773.

References

Ballard, K. R., Mead, A. R. G., Brand, P. W. J. L., et al. 1990, MNRAS, 243, 640
Bersanelli, M., Bouchet, P., Falomo, R., et al. 1992, AJ, 104, 28
Bessell, H. S. 1979, PASP, 91, 589
Brown, I. M. J., Robson, E. I., Gear, W. K., et al. 1989, ApJ, 340, 129
Cardelli, J. A., Clayton, G. C., & Mathis, J. S. 1989, ApJ, 345, 245
Chiang, J., & Böttcher, M. 2002, ApJ, 564, 92
Ciprini, S., Tosti, G., Raiteri, C. M., et al. 2003, A&A, 400, 487
Ciprini, S., Tosti, G., Teräsranta, H., & Aller, H. D. 2004, MNRAS, accepted
Donato, D., Ghisellini, G., Tagliaferri, G., et al. 2001, A&A, 375, 739
Elvis, M., Lockman, F. J., & Wilkes, B. J. 1989, AJ, 97, 777
Falomo, R., Bersanelli, M., Bouchet, P., et al. 1993, AJ, 106, 11
Fan, J., & Lin, R. 1996, Publ. Yunnan Obs., 4, 8
Fan, J., Feng, X., & Su, C. 1999, Publ. Yunnan Obs., 77, 1
Fiorucci, M. 1995, Ph.D. Thesis
Fiorucci, M., & Tosti, G. 1996, A&AS, 116, 403
Fiorucci, M., Tosti, G., & Rizzi, N. 1998, PASP, 110, 105
Ghisellini, G., Celotti, A., & Costamante, L. 2002, A&A, 386, 833
Giommi, P., Capalbi, M., Fiocchi, et al. 2002, in Blazar Astroph. with BeppoSAX & Other Obs., ASI Publ., 63
Gonzalez-Pérez, J. N., Kidger, M. R., & Martin-Luis, F. 2001, AJ, 122, 2055
Idesawa, E., Tashiro, M., Makishima, K., et al. 1997, PASJ, 49, 631
Kataoka, J., Takahashi, T., Makino, F., et al. 2000, ApJ, 528, 243
Kirk, J. G., & Mastichiadis, A. 1999, Astropart. Phys., 11, 45
Kirk, J. G., Rieger, F. M., & Mastichiadis, A. 1998, A&A, 333, 452
Lamer, G., Brunner, H., & Staubert, R. 1996, A&A, 311, 384
Landau, R., Golish, B., Jones, T. J., et al. 1986, ApJ, 308, 78
Ledden, J. E., & O'Dell, S. L. 1985, ApJ, 298, 630
Maraschi, L., Fossati, G., Tavecchio, F., et al. 1999, ApJ, 526, L81
Massaro, E., Giommi, P., Perri, M., et al. 2003, A&A, 399, 33
Massaro, E., Nesci, R., Maesano, M., et al. 1996, A&A, 314, 87
Massaro, E., & Trèvese, D. 1996, A&A, 312, 810
Padovani, P., & Giommi, P. 1995, ApJ, 444, 567
Pian, E., Falomo, R., Scarpa, R., et al. 1994, ApJ, 432, 547
Pian, E., Vacanti, G., Tagliaferri, G., et al. 1998, ApJ, 492, L17
Raiteri, C. M., Villata, M., Tosti, G., et al. 1999, A&A, 352, 19
Reuter, H.-P., Kramer, C., Sievers, A., et al. 1997, A&AS, 122, 271
Roy, M., Papadakis, I. E., Ramos-Colón, E., et al. 2000, ApJ, 545, 758
Scarpa, R., Urry, C. M., Falomo, R., et al. 2000, ApJ, 532, 740
Schlegel, D. J., Finkbeiner, D. P., & Davis, M. 1998, ApJ, 500, 525
Sembay, S., Warwick, R. S., Urry, C. M., et al. 1993, ApJ, 404, 112
Smith, P. S., Balonek, T. J., Elston, R., et al. 1987, ApJS, 64, 459
Smith, P. S., & Balonek, T. J. 1998, PASP, 110, 1164
Spada, M., Ghisellini, G., Lazzati, D., & Celotti, A. 2001, MNRAS, 325, 1559
Tagliaferri, G., Ghisellini, G., Giommi, P., et al. 2000, A&A, 354, 431
Tagliaferri, G., Ravasio, M., Ghisellini, G., et al. 2003, A&A, 400, 477
Takahashi, T., Kataoka, J., Madejski, G., et al. 2000, ApJ, 542, L105
Takalo, L. O., Sillanpää, A., Pursimo, T., et al. 1996, A&AS, 120, 313
Tosti, G., Fiorucci, M., Luciani, M., et al. 1998, A&A, 339, 41
Tosti, G., Massaro, E., Nesci, R., et al. 2002, A&A, 395, 11
Tosti, G., Pascolini, S., & Fiorucci, M. 1996, PASP, 108, 706
Trèvese, D., & Vagnetti, F. 2002, ApJ, 564, 624
Türler, M., Paltani, S., Courvoisier, T. J., et al. 1999, A&AS, 134, 89
Urry, C. M., Scarpa, R., O'Dowd, M., et al. 2000, ApJ, 532, 816
Vagnetti, F., Trèvese, D., & Nesci, R. 2003, ApJ, 590, 123
Véron-Cetty, M.-P., & Véron, P. 2001, A&A, 374, 92
Webb, W., & Malkan, M. 2000, ApJS, 130, 165
Wehrle, A. E., Pian, E., Urry, C. M., et al. 1998, ApJ, 497, 178